THE ASTROPHYSICAL JOURNAL, 420:143–151, 1994 January 1

X-RAY CONTINUUM AND IRON K EMISSION LINE FROM THE RADIO GALAXY 3C 390.3

M. INDA,[1] K. MAKISHIMA,[1] Y. KOHMURA,[1] M. TASHIRO,[1] T. OHASHI,[2] P. BARR,[3] K. HAYASHIDA,[4]
G. G. C. PALUMBO,[5] G. TRINCHIERI,[6] M. ELVIS,[7] AND G. FABBIANO[7]
Received 1993 February 8; accepted 1993 July 8

ABSTRACT

X-ray properties of the radio galaxy 3C 390.3 were investigated using the *EXOSAT* and *Ginga* satellites. Long-term, large-amplitude X-ray intensity changes were detected over a period extending from 1984 through 1991, and high-quality X-ray spectra were obtained especially with *Ginga*. The X-ray continuum spectra were described with power-law model with photon slope in the range 1.5–1.8, and the slope flattened as the 2–20 keV luminosity decreased by 40%. There was a first detection of the iron emission line from this source at the 90% confidence level. An upper limit was derived on the thermal X-ray component. X-ray emission mechanisms and possible origins of the long-term variation are discussed.

Subject headings: galaxies: individual (3C 390.3) — galaxies: active — X-rays: galaxies

1. INTRODUCTION

Radio galaxies occupy an important position as a possible parent population for quasars (QSOs) and BL Lac objects (Brown & Murphy 1987; Barthel 1989). In fact, certain models (called "Unified Scheme"; see Orr & Brown 1982) claim that a group of radio galaxies that are seen nearly end-on to their radio jets should become a highly relativistically beamed luminous class of active galactic nuclei (AGNs). In order to test the Unified Scheme, it is important to better understand the X-ray characteristics of radio galaxies and compare them with those of other types of AGN, because X-ray emission is thought to be directly related to the emission mechanism of the central engine of the AGN.

3C 390.3 is a broad-line radio galaxy at $z = 0.057$. In the radio, it is classified as F-R II (lobes with leading edge hot spots; Fanaroff & Riley 1974), and has a prominent double-lobed morphology, together with a compact nucleus which shows evidence of superluminal motion (Alef et al. 1988). The optical spectrum, which classifies it as an N galaxy (Burbidge & Burbidge 1971; Penston & Penston 1973), shows broad Hα and Hβ lines whose double-peaked structure provides evidence for an accretion disk (Perez et al. 1988). Since its first X-ray detection by *Uhuru* (Giacconi & Gursky 1974; Forman et al. 1978), 3C 390.3 has also been known to have an X-ray luminosity as large as $L_X \sim 10^{44}$ ergs s^{-1}. The galaxy has been subsequently monitored in X-rays by several satellites, up to the most recent observations with *EXOSAT* (Shafer, Ward, & Barr 1985, hereafter SWB85), and the new results from *Ginga* that we are presenting here. The *HEAO 1* data indicate X-ray spectra of power-law form with photon index $\Gamma = 1.65\,(+0.50, -0.25)$ in 2–50 keV (error is 90% confidence level) and $\Gamma = 1.40 \pm 0.37$ in 12–165 keV (error is 1 σ uncertainty) (Rothschild et al. 1983; Mushotzky 1984), which are typical of an AGN, and has a 2–10 keV luminosity of $L_X = 10^{43.8}$ ergs s^{-1}. A continuous decline of 3C 390.3 has been observed over a period of $\sim$15 yr up to $\sim$1984, in the optical blue continuum (from 14.8 to 16.6 mag; Barr et al. 1980; Lloyd 1984; SWB85), in the optical broad-line components (Oke 1986), in ultraviolet lines (Clavel & Wamsteker 1987), and in X-rays (SWB85).

Here we report on the X-ray observations of 3C 390.3 made with the *EXOSAT* and *Ginga* satellites, and present high-quality X-ray spectra obtained with *Ginga*. In § 2 and § 3 we describe our observations and results respectively, followed by the discussion in § 4.

2. OBSERVATIONS

2.1. *EXOSAT Observations*

A total of six *EXOSAT* observations of 3C 390.3 were performed between 1984 and 1986. Data from the first two observations have already been reported (SWB85); processed data from all six observations are publicly available in the *EXOSAT* data base. However, for a weak source like 3C 390.3, where the hard X-ray data are background-noise dominated, it is often possible to obtain significantly better reduced data than available in the archive by interactive reanalysis of the raw data. Therefore, we have systematically reanalyzed all data from the Medium Energy proportional counter array (ME; Turner, Smith, & Zimmerman 1981) to obtain a uniform sample of X-ray spectra.

Observations were performed on 1984 day 153, day 259; 1985 day 33, day 311; and 1986 day 76, day 77. Both observations in 1984 were affected by solar activity; on day 153, 63 minutes of data were not used due to background variations, while on day 259 the ME data were completely unusable due to solar flaring. We therefore exclude 1984 day 259 data from the present analysis. The useful data on 1985 day 33 were truncated by 3 hours due to spacecraft pointing problems. Only 54 minutes of useful data were obtained on 1985 day 311 due to background variations.

The ME was usually operated with one-half of the detector array pointed at the source and the other offset at a blank

[1] Department of Physics, University of Tokyo, 7-3-1 Hongo, Bunkyo-ku, Tokyo, Japan 113.
[2] Department of Physics, Tokyo Metropolitan University, 1-1 Minami-Osawa, Hachioji, Tokyo, Japan 192-03.
[3] *EXOSAT* Observatory, Astrophysics Divisions, Space Science Department, ESTEC, NL-2200 AG Noordwijk, The Netherlands.
[4] Department of Earth and Space Science, Osaka University, 1-1 Machikane-yama, Toyonaka, Osaka, Japan 560.
[5] Dipartimento di Astronomia, Università di Bologna, Via Zamboni 33, 40126 Bologna, Italy.
[6] Osservatorio Astrofisico di Arcetri, Largo Enrico Fermi 5, 50125 Firenze, Italy.
[7] Harvard-Smithsonian Center for Astrophysics, 60 Garden Street, Cambridge, MA 02138.

region of the sky, to measure the detector background, the two halves being exchanged at mid-observation. However, for the 1984 day 153 and 1985 day 311 observations, significantly better background subtraction was obtained using data from the slews onto and off the target.

2.2. *Ginga Observations*

We observed 3C 390.3 with the *Ginga* LAC (Large area Proportional Counter; Turner et al. 1989) in the pointing mode on two occasions; 1988 November 12 (=day 316) 2:02–22:53 UT and November 13 (=day 317) 0:14–17:14 UT, and 1991 February 14 (=day 45) 9:10–23:08 UT. We accumulated $\sim 3 \times 10^4$ s and 1.5×10^4 s of net on-source exposure, for the 1988 and 1990 observations, respectively. The background data were obtained on 1988 November 11 at $(\alpha^{1950}, \delta^{1950}) = (18^h30^m.8, 81°28'.8)$, 1°.9 off 3C 390.3, and on 1991 February 13 at $(16^h23^m.1, 76°15'.6)$, 8°.0 off. We performed no scanning observations which are sometimes done to obtain estimates of contamination from nearby sources, since, upon examination of the *Einstein* Extended Medium Sensitivity Survey (Gioia et al. 1991), we expect negligible contribution from other sources in the same field of view. During these observations events from each of the LAC detectors were pulse-height analyzed and accumulated on board into 48 spectral channels covering an energy range of 1–36 keV, with time resolution of either 4 or 16 s (MPC-1 mode).

Significant source flux was detected in both observations. The background-subtracted and aspect-corrected 2–20 keV signal counting rate was ~ 24 counts s^{-1} and ~ 13 counts s^{-1} in the first and second observation, respectively. Note that a 1 mCrab flux corresponds to ~ 10 counts s^{-1} (2–20 keV) in the *Ginga* LAC. These values are subject to a statistical error of ~ 0.05 counts s^{-1} for a 1 day long observation, and a systematic source confusion noise of 1.4 counts s^{-1} (both 2–20 keV, at the 90% confidence; Hayashida et al. 1989). Figure 1 shows the background-subtracted light curve, binned at 128 s. The LAC counting rates remained constant within $\sim 5\%$ within each day of observation, but the average X-ray intensity decreased from 26 counts s^{-1} to 23 counts s^{-1} by 3 ± 1 counts s^{-1} between the 2 days in 1988. This decrease is significant compared with the statistical errors, as well as the background and aspect uncertainties.

Toward the end of the second *Ginga* observation, namely at 22:29 UT on 1991 February 14, a prominent flare event was detected. During the flare, which lasted for ~ 30 minutes until the end of the observation, the LAC counting rate increased by a factor of 10 (Fig. 1*c*). We describe this event in detail in § 3.3, where we argue that the flare is due to a dMe star in the same field of view and that "quiescent" emission from the flare

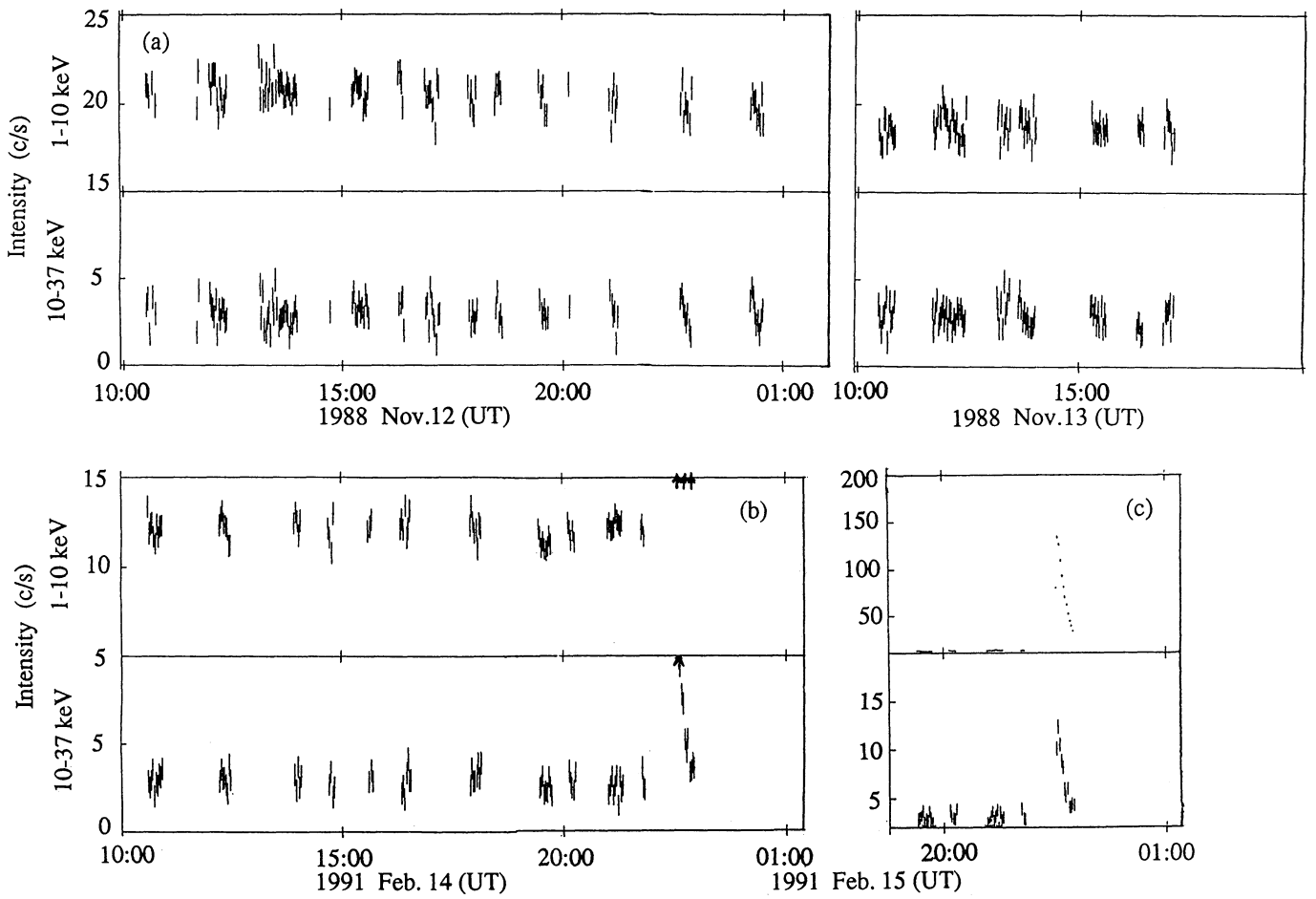

FIG. 1.—The two-color X-ray light curves of 3C 390.3 obtained by *Ginga*. (*a*) 1988 November observation. (*b*) 1991 February observation; as discussed in the text, a large flare-like event occurred at about 22:29 UT on February 14. The flare position is replotted in (*c*) with compressed flux scales.

TABLE 1

X-RAY FLUXES AND LUMINOSITIES OF 3C 390.3 OBSERVED WITH *EXOSAT* AND *Ginga*[a]

SATELLITE	YEAR/DAY	Γ[b]	2–6 keV FLUX[c]	LUMINOSITY[d] 2–6 keV	LUMINOSITY[d] 2–20 keV
EXOSAT	1984/153	(1.7)	0.28 ± 0.03	0.10 ± 0.01	0.25 ± 0.03
EXOSAT	1985/033	(1.7)	1.75 ± 0.05	0.61 ± 0.02	1.56 ± 0.04
EXOSAT	1985/311	(1.7)	1.44 ± 0.07	0.50 ± 0.02	1.28 ± 0.06
EXOSAT	1986/076	(1.7)	1.26 ± 0.03	0.44 ± 0.01	1.12 ± 0.03
EXOSAT	1986/077	(1.7)	1.27 ± 0.04	0.44 ± 0.01	1.13 ± 0.03
Ginga	1988/316	1.79 ± 0.02	3.11 ± 0.08	1.09 ± 0.03	2.60 ± 0.06
Ginga	1988/317	1.76 ± 0.02	2.84 ± 0.08	0.99 ± 0.03	2.43 ± 0.07
Ginga	1991/045	1.54 ± 0.02	1.62 ± 0.05	0.57 ± 0.02	1.62 ± 0.05

[a] All the errors are 90% confidence limits.
[b] Photon index of the power-law spectrum. It was fixed at 1.7 for the *EXOSAT* data.
[c] Calculated using the power-law fits and expressed in units of 10^{-11} ergs cm^{-2} s^{-1}.
[d] In units of $10^{44}\ h^{-2}$ ergs s^{-1}.

source is negligible. Therefore, the analysis of the *Ginga* data will not cover the flare period.

3. RESULTS

3.1. *X-Ray Intensity*

The X-ray fluxes observed with *EXOSAT* and *Ginga* are shown in Table 1, together with the luminosities calculated for a distance of $D = 171\ h^{-1}$ Mpc (for $H_0 = 100h$ km s^{-1} Mpc^{-1}). Here 2–6 keV fluxes of the *EXOSAT* observations were calculated from the observed 2–10 keV ME spectrum, in which the photon index Γ was fixed at 1.7. Leaving Γ to vary freely resulted in consistent flux values within errors (see § 3.2). The photoelectric absorption was assumed to be negligible, because for all the *EXOSAT* spectrum it is consistent with zero (see § 3.2) and did not affect the calculation in the 2–6 keV flux.

In Figure 2, we compare these 2–6 keV intensity measurements with previous X-ray observations of 3C 390.3. The figure clearly reveals a large amplitude (more than an order of magnitude even excluding the single Copernicus point which is rather uncertain) X-ray variation on a time scale of 10 ~ 20 yr; following the long-term decline over 1973–1984 (Barr et al. 1980; SWM85), the X-ray intensity has been increasing in the years 1984–1989. The X-ray flux also exhibits a factor ~3 random variability on somewhat shorter time scales (a few years). It is thus not obvious whether the flux decrease from 1988 to 1991 signals the start of another long-term source decline, or just a short-term fluctuation.

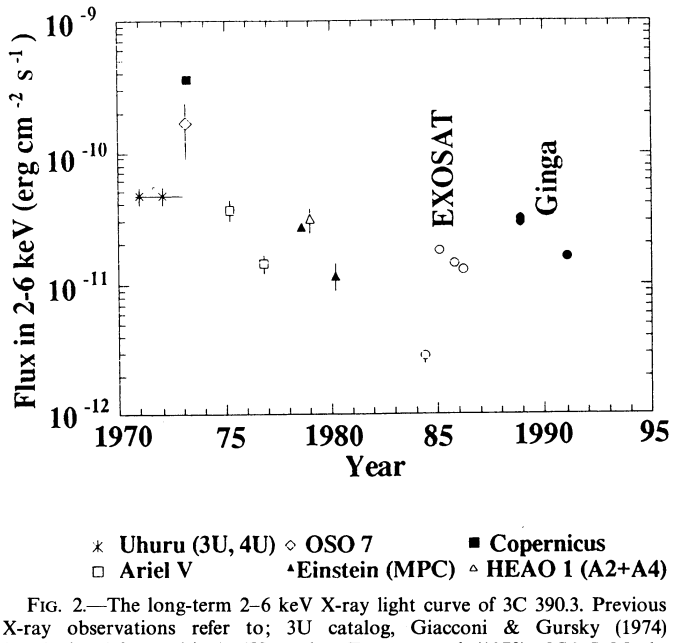

FIG. 2.—The long-term 2–6 keV X-ray light curve of 3C 390.3. Previous X-ray observations refer to; 3U catalog, Giacconi & Gursky (1974) (recalculated for position); 4U catalog, Forman et al. (1978); *OSO 7*, Mushotzky et al. (1977); *Copernicus*, Charles et al. (1975); *Ariel 5*, Barr et al. (1980); *HEAO 1*, Marshall et al. (1978), Rothschild et al. (1983), and Wood et al. (1984); *Einstein*, Halpern (1982). The *OSO 7* flux was calculated assuming a power-law model with photon index $\Gamma = 1.7$.

3.2. *EXOSAT Spectra*

A series of trial power-law spectra were folded through the detector response and fitted to the ME data at each epoch. Results are given in Table 2. The photoelectric absorption is included as a free parameter in the fits to the *EXOSAT* data. In all cases it is consistent with zero. For the 1984 day 153 observations, SWB85 reported a flat X-ray power law with little or no absorption. In our reanalysis, the derived *best-fit* spectrum is steep. However, the uncertainty in the spectral index is quite large. In fact, there is no evidence that the spectral index measured by *EXOSAT* is variable. The hypothesis of constant spectral index yields a reduced χ^2 of 0.84 for four d.o.f. The (weighted) mean 2–10 keV spectral index measured by *EXOSAT* is 1.66, typical of hard X-ray power laws for AGNs (Turner & Pounds 1989).

Addition of a Gaussian emission feature near 6.4 keV yields no significant decrease in χ^2; however, the upper limits to the strength of any iron line are uninteresting, 3 σ limits to the equivalent width in all observations being in excess of 600 eV.

3.3. *Ginga Spectra*

3.3.1. *Continuum Characteristics*

The two *Ginga* observations yielded high-quality X-ray spectra in the 2–36 keV range, as shown in Figure. 3. The data have been background subtracted (using the standard method by Hayashida et al. 1989) and aspect corrected, but the detector response has not been removed. The 1991 spectrum (Fig. 3*b*) excludes the period of the flare event (§ 2.2).

We fitted the spectra with power-law and thermal bremsstrahlung models with three free parameters; normalization factor, photon index Γ or temperature kT, and absorption by cold matter of cosmic abundance with a column density N_H.

TABLE 2

RESULTS OF MODEL FITS TO THE 3C 390.3 SPECTRA[a]

Year/Day	Model	N_0[b]	Γ[c] or kT[d]	$E_C(1+z)$[e]	EW[f]	χ^2/d.o.f.[g]
1984/153	Power law	$2.9(+3.3, -1.4)$	2.5 ± 0.7	...	...	27/18
1985/033	Power law	5.1 ± 1.5	1.75 ± 0.2	...	...	37/35
1985/311	Power law	5.7 ± 1.2	1.7 ± 0.2	...	...	26/32
1986/076	Power law	4.4 ± 0.1	1.6 ± 0.1	...	...	27/32
1986/077	Power law	4.3 ± 0.5	1.57 ± 0.08	...	...	21/36
1988[h]	Power law	12.9 ± 0.27	1.77 ± 0.01	...	...	40.1/37
	Thin-thermal	17.3 ± 0.17	14.2 ± 0.4	...	...	333/37
	Power law + line	12.9 ± 0.28	1.77 ± 0.01	6.60 ± 0.35	70 ± 36	30.9/35
1991/045	Power-law	5.13 ± 0.16	1.54 ± 0.02	...	...	45.0/35
	Thin thermal	9.28 ± 0.09	27.2 ± 2.0	...	...	55.7/35
	Power law + line	5.13 ± 0.16	1.54 ± 0.02	6.49 ± 0.37	96 ± 56	36.2/35

[a] Errors represent single-parameter 90% confidence levels.
[b] Normalization (10^{-3} counts s^{-1} keV^{-1} cm^{-2}).
[c] Photon index.
[d] Thermal bremsstrahlung temperature (keV).
[e] Line center energy (keV) with redshift correction assuming $z = 0.057$.
[f] Line equivalent width (eV).
[g] Degree of Freedom.
[h] The 2 day long *Ginga* data were combined together.

Results of the fitting in Table 2 show that the power-law model is clearly more favored than the thermal model for the 1988 data, although in the 1991 data the distinction between the two models is less clear and even the power-law fit gives somewhat large chi-squared. As shown in Figure 4*a*, we obtained only upper limits to N_H which are consistent with the line-of-sight absorbing column within our galaxy, in this direction of the sky (3×10^{20} cm^{-2}; Heiles & Habing 1974).

One intriguing result is the detection of a significant change, by ~ 0.23, in the photon index Γ between the two *Ginga* observations (see Table 2). As shown by the contour map of Figure 4*a*, this spectral difference is statistically significant. The differ-

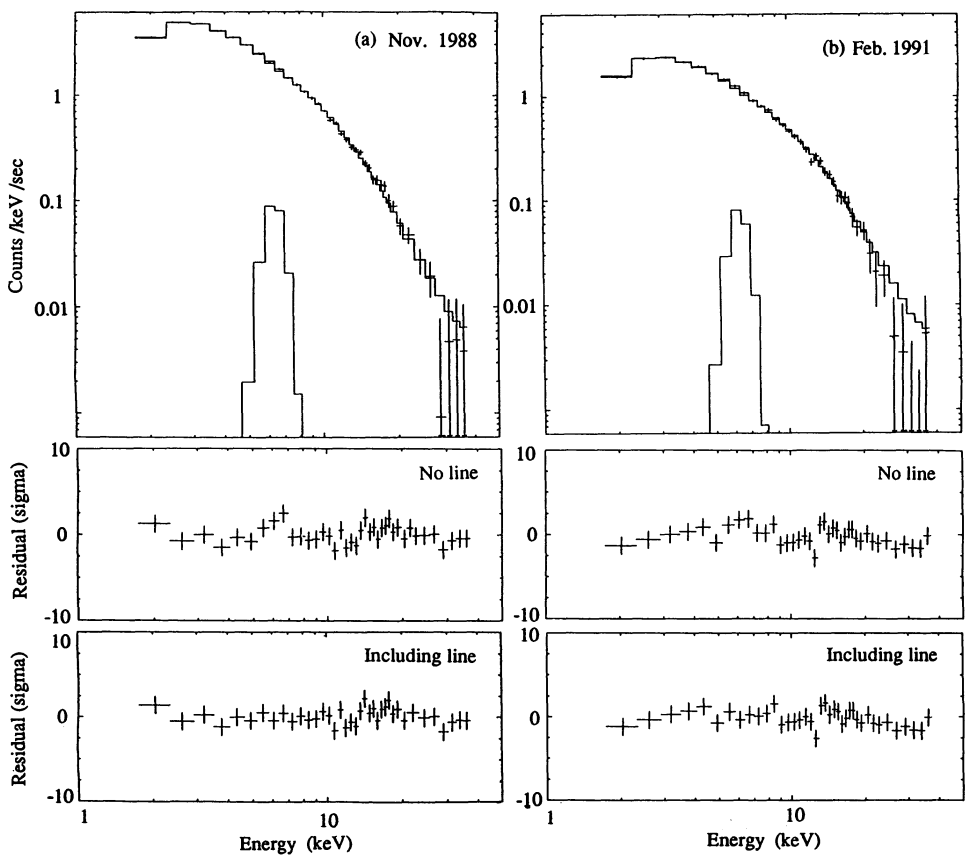

FIG. 3.—X-ray spectra of 3C 390.3 obtained in the first (*a*) (total 23.5 counts s^{-1}) and the second (*b*) (total 13.4 counts s^{-1}) *Ginga* observations. Top panels display X-ray pulse-height spectra (*cross*) without removing instrumental response, in comparison with the best-fitting power-law plus iron emission line models (*solid line*). Middle panels are residuals from the single power-law fits, while bottom panels show those from the power-law plus iron emission line models. The best-fit model parameters are summarized in Table 2.

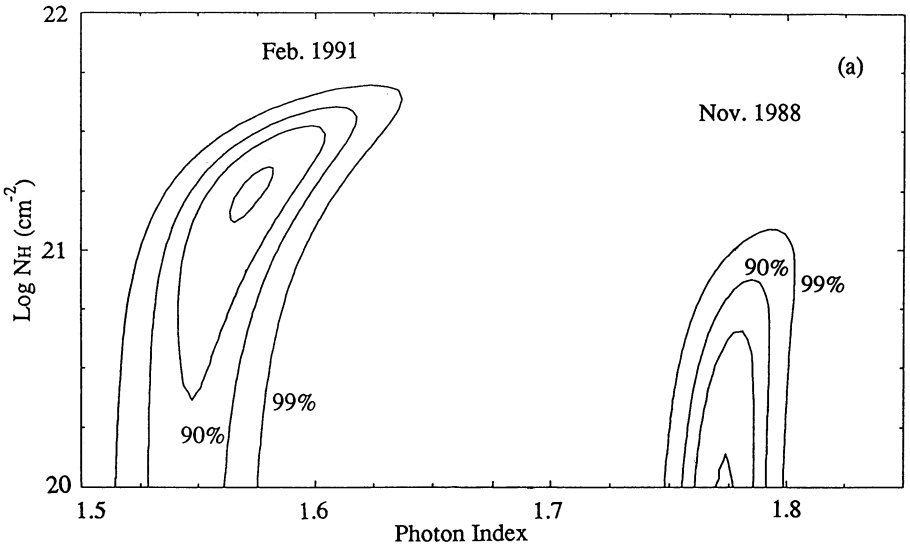

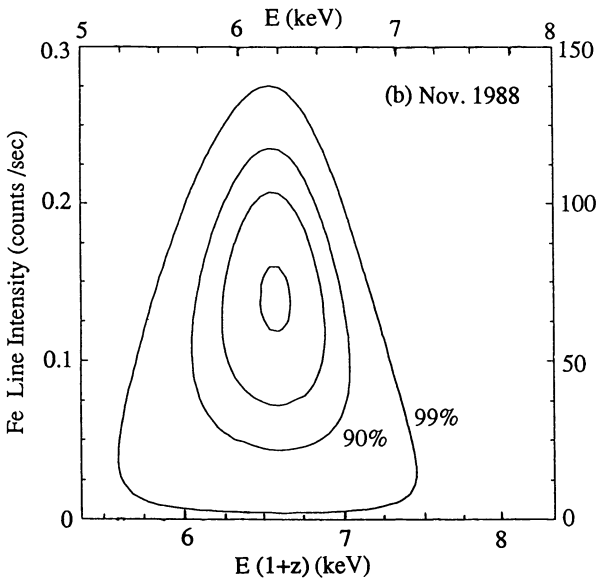

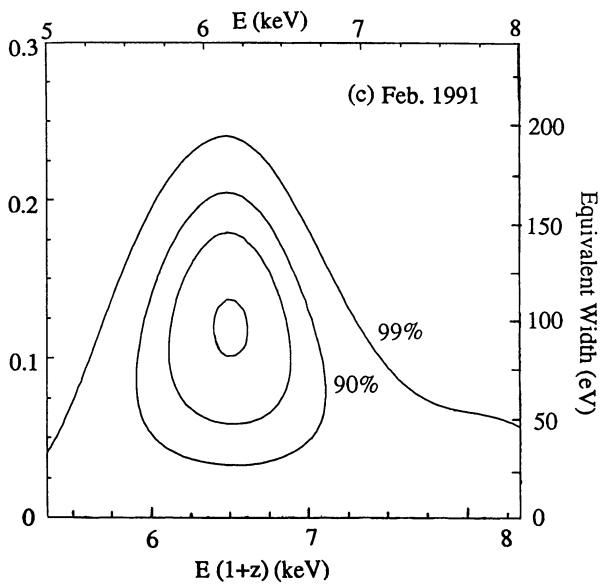

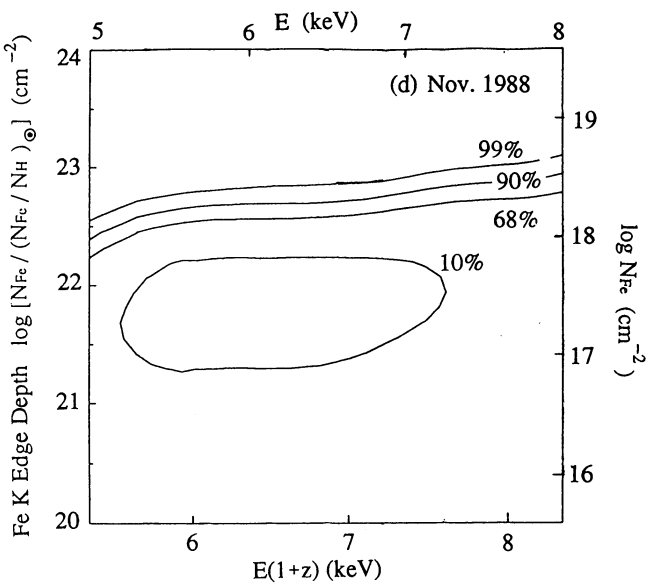

FIG. 4.—The confidence contours for the *Ginga* spectral parameters. Confidence levels are 99.0%, 90.0%, 68.0%, and 10.0%. (*a*) Photon index vs. absorption for the power-law continuum. (*b*) and (*c*) Iron line intensity (or equivalent width) vs. line center energy, obtained with power law plus Gaussian emission line model. (*d*) Constraints on the iron K-edge absorption feature for the 1988 data, displayed against the assumed iron K-edge energy.

ence is also much larger than the systematic errors (mainly due to background uncertainties) in Γ, which is no larger than ± 0.05 in the present case. We further searched the *Ginga* data for fast spectral changes on time scales of minutes to days, but none was found. In particular, the first and second day of the 1988 observation yielded the same value of Γ within errors of ± 0.03.

3.3.2. *Iron* K-*Emission Line and Iron* K-*Edge Feature*

The single power-law fits to the *Ginga* spectra exhibit a hint of positive residual around 6 keV (Fig. 3, middle panels). This suggests the existence of a redshifted iron K-emission line. We accordingly added to the power-law model a narrow (0.1 keV FWHM) Gaussian component, leaving its intensity and center energy free to vary. This significantly improved the χ^2 of the fit (Table 2 and the bottom panels of Fig. 3). Confidence contour maps for the Gaussian parameters, Figure 4*b* and 4*c*, show evidence of line emission in both spectra. Also, F-tests confirm the line significance at a 99.9% confidence level for the 1988 observation and at a 99.0% confidence level for the 1991 observation. The derived line-center energies, after correction for $z = 0.057$, are consistent with those of iron K-lines (6.4–6.93 keV in the rest frame). We therefore conclude that the *Ginga* spectra provide the first significant evidence of the iron K-line emission from 3C 390.3, with equivalent width (EW) of ~ 100 eV. In a later discussion (§ 3.3.3) we show that the iron line is unlikely to originate in the contaminating flare source. We cannot, however, constrain the line energy enough to determine, within the 90% confidence levels, whether the inferred iron line is of fluorescent origin (expected at 6.4 keV in the rest frame) or of thermal origin (expected at 6.7–6.9 keV in the rest frame). Also, we cannot discriminate between the line flux or the line EW being the same between the two observations.

Motivated by a series of *Ginga* detections of iron K-edge features from many Seyfert galaxies (e.g., Pounds et al. 1990; Matsuoka et al. 1990), we examined the 3C 390.3 spectra for similar iron K-edge absorption features. We multiplied the power-law model by the K-edge absorption factor and varied both the edge energy and depth in comparison with the data. However, no edge feature was detected from either spectrum of 3C 390.3, and the derived upper limits on the iron column density are of order 4×10^{18} cm^{-2} as shown in Figure 4*d*, corresponding to an equivalent hydrogen column of 1×10^{23} cm^{-2} assuming cosmic abundance.

3.3.3. *Origin of the X-Ray Flare and Its Effects on the Ginga Data*

In this subsection we will discuss the flare in the second *Ginga* observation and justify the exclusion of these data from the analysis. The flare is due to valid aperture X-rays, because background monitor counts (Hayashida et al. 1989) did not increase. The flare exhibited a rapid (5 minutes) tenfold flux rise followed by a ~ 30 minutes decay, although the observation ended before the flux recovery to the preflare level. We derived X-ray spectra of the flare component, in time series, by subtracting preflare data including both background and the 3C 390.3 signal. These flare spectra are well fitted with thermal bremsstrahlung continuum, plus an iron emission line with a center energy of 6.7 ± 0.1 keV and an EW in the range 600–1400 eV. Fitting with the Raymond-Smiths (1977) model resulted in consistent parameter values. The continuum temperature gradually decreased from $kT = 10$ keV (flare peak) to 4 keV. The flare spectra cannot be fitted with power law plus line model.

From the spectral analysis, it is most likely that the flare X-rays are emission from optically thin hot plasma, whose size is at most 10^{13} cm corresponding to the flare rise time. Any detectable thin-thermal emission associated with the radio galaxy would not exhibit such a rapid variation (Elvis et al. 1991). We can also exclude a solar origin, since, during the flare, the LAC field of view was clear from direct solar illumination and terrestrial scattering of solar X-rays. On the other hand, this event is very reminiscent of solar and late-type stellar X-ray flares (e.g., Haish 1983; Tsuru et al. 1989; Pallavicini, Tagliaferri, & Stella 1990). We therefore suggest that a dMe star EQ 1839.6+8002 (Caillaut et al. 1986), only 0°.4 away from 3C 390.3, to be the flare source. The estimated distance of $D = (11$–$40)$ pc to this star implies a 2–10 keV flare peak luminosity of 1.3×10^{30} $(D/10$ pc$)^2$ ergs s^{-1}. This value is consistent with those of dMe flares. Further details of this event will be reported elsewhere.

The flare source was in the LAC field of view throughout both observations, and we must estimate its contribution during its quiescent state for possible contamination. Because the X-rays from 3C 390.3 are of nonthermal nature (§3.3.1), the amount of thermal component allowed by the *Ginga* spectra is expected to set an upper limit on the contamination. We accordingly fit the 3C 390.3 spectra (Fig. 3) with a model consisting of power-law and thermal bremsstrahlung continua (both without absorption), leaving all the continuum parameters free while masking out the iron line region (5.8–7.0 keV). The upper limit on the thermal flux thus constrained is shown in Figure 5*a* as a function of the assumed bremsstrahlung temperature. The result indicates that thermal flux is at most $\sim 8\%$ of the total flux in both spectra, or less than $(3.9$–$5.8) \times 10^{-12}$ ergs cm^{-2} s^{-1}, for coronal temperatures below ~ 4 keV (assuming that the coronal temperature is lower in quiescence than during flares). This is consistent with the IPC flux of EQ 1839.6+8002, which is 7.8×10^{-13} ergs cm^{-2} s^{-1} in 0.15–4 keV (Caillaut et al. 1986). The above results imply that the flare peak luminosity is at least 10^3 times larger than the quiescent X-ray luminosity of the flare source. This is not unusual for late-type flare stars. From these arguments, we conclude that the contamination to the continuum emission by the quiescent stellar emission is negligible.

To examine whether the iron line emission comes from the flare star or from the radio galaxy, we have calculated the maximum iron line EW (relative to the observed total continuum) attributable to the quiescent stellar emission, by utilizing the upper limit on the thermal continuum (Fig. 5*a*) and the iron line EW (relative to the calculated thermal continuum) expected for a plasma of solar abundance (Rothenflug & Arnaud 1985). The result, shown in Figure 5*b*, indicates that the estimated upper limits on the stellar line EW are comparable to those actually observed in the 3C 390.3 spectra. However, the redshift-uncorrected line energies for the 3C 390.3 spectra, 6.24 ± 0.33 keV (in 1988) and 6.14 ± 0.35 keV (in 1991), are inconsistent with the energy of ~ 6.7 keV expected for stellar coronae of temperature $kT = 2$–10 keV, which has actually been observed in the flare X-rays. (Note that the line energies observed from 3C 390.3 become consistent with either 6.7 or 6.4 keV after the redshift correction.) We therefore conclude that the quiescent stellar emission cannot be a main source of the detected iron K-line photons.

3.3.4. *Upper Limits on the Thermal Component*

X-ray bright elliptical galaxies are surrounded by hot ($kT \sim 1$ keV) gaseous halos which emit thermal X-rays with luminosities in the range 10^{41}–10^{42} ergs s^{-1} (Forman, Jones, & Tucker 1985; Canizares, Fabbiano, & Trinchieri 1987; Fabbiano, Kim, & Trinchieri 1992). In radio galaxies, hydrostatic pressure of such a hot halo may significantly contribute to the confinement of the radio lobes. The analysis conducted in the preceding subsection is particularly useful in setting upper limits on possible thermal X-ray emission from such an extended gaseous halo in the 3C 390.3 system. Assuming that thermal flux should not vary and therefore combining the two results in Figure 5*a*, 2–20 keV thermal flux from 3C 390.3 itself can be constrained to less than 4×10^{-12} ergs s^{-1} cm^{-2} for $kT < 10$ keV, corresponding to a 2–20 keV luminosity of less than $1h^{-2} \times 10^{43}$ ergs s^{-1} (<5% of the total luminosity seen in *Ginga*). The upper limit is further reduced for lower temperatures, e.g., less than $2h^{-2} \times 10^{42}$ and less than $1h^{-2} \times 10^{42}$ ergs s^{-1} for $kT = 3$ and 2 keV, respectively.

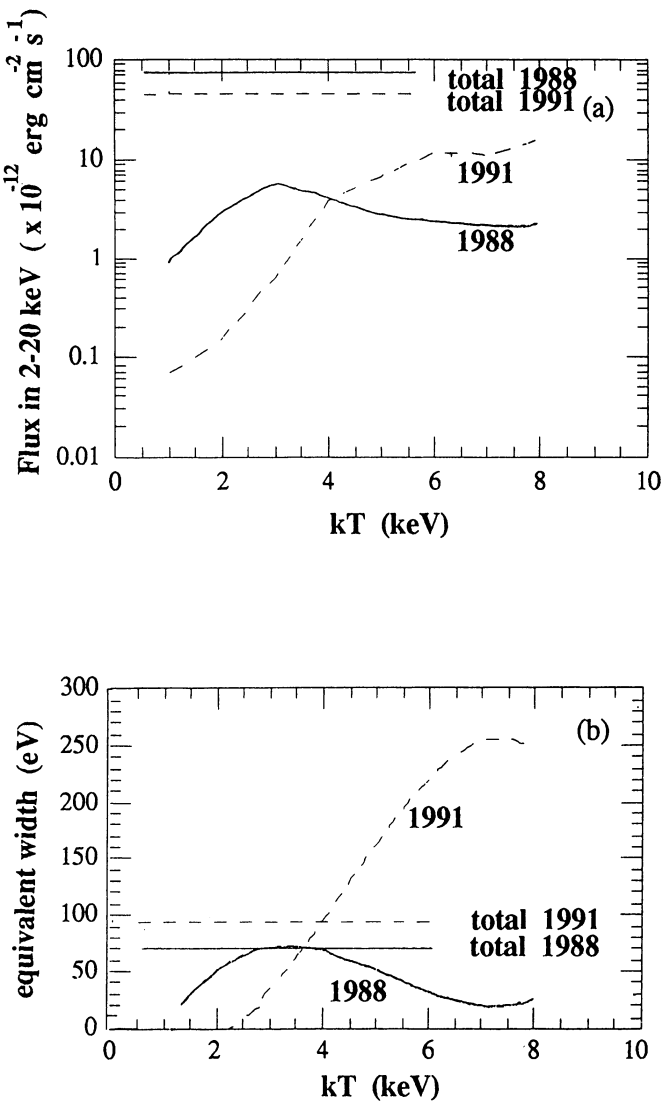

FIG. 5.—(*a*) Upper limits (90% confidence level) on the 2–20 keV thermal continuum flux allowed by the *Ginga* spectra of 3C 390.3. The total 2–20 keV *Ginga* fluxes are also shown. (*b*) Upper limits (90% confidence level) on thermal iron K-emission line equivalent width (with respect to the observed total continuum) expected for a solar-abundance plasma in ionization equilibrium whose continuum flux is constrained by (*a*). The straight lines indicate actually observed equivalent widths.

4. DISCUSSION

4.1. *Long-Term Variability*

Over the period of ~1970 to mid 1980s, 3C 390.3 exhibited a long-term decline in its optical blue continuum, optical broad-line components, and X-rays (Barr et al. 1980; van Breugel & Jagers 1982; Lloyd 1984; Laing, Riley, & Longair 1983; SWB85). The X-ray observations from *EXOSAT* and *Ginga* have shown an increase, from the minimum in 1984 May to a peak in 1988 November, by almost an order of magnitude. This is one of the largest amplitude variations in X-rays observed in AGNs (see Grandi et al. 1992). The *IUE* observations made in 1989 March (Wamsteker & Clavel 1989) also reported a marked increase in the ultraviolet continuum and lines of 3C 390.3 (doubling of the continuum, a 70% and a 160% increase in the Lyα and C IV line, respectively) with respect to the observation in early 1988.

These results immediately indicate that thermal or inverse-Compton X-ray emission from large extended regions, including the radio lobes, and hot plasmas which might be necessary to confine the radio lobes, is at most $3h^{-2} \times 10^{43}$ ergs s^{-1} in 2–20 keV corresponding to the minimum intensity observed on 1984 day 153. All the variable X-ray flux, with luminosities reaching $\sim 2.5h^{-2} \times 10^{44}$ ergs s^{-1}, must originate in the compact nucleus. This conclusion is quite consistent with the fact that the *Ginga* spectra are clearly of a nonthermal nature with characteristics very similar to those of other AGNs, and that the allowed thermal X-ray luminosity is less than $1h^{-2} \times 10^{43}$ ergs s^{-1} (Fig. 5*a*) for a rather wide range of assumed temperature ($kT = 2$–10 keV).

There are several alternative interpretations for the cause of the observed X-ray variability. One obvious possibility is a real change in the intrinsic luminosity of the nucleus. Changes in the nuclear obscuration by cold matter can also cause apparent X-ray intensity changes, and this is actually suggested by the reduced optical broad lines during the low flux period. Also evidence was reported previously for occasional variation in the X-ray absorption (Charles, Longair, & Sanford 1975). However, a tenfold intensity reduction in the *EXOSAT* ME range by increased absorption would have required an equivalent hydrogen column density in excess of 3×10^{23} cm^{-2}, which would have caused a serious change in the ME spectrum. Since such a drastic spectral change was not observed the increased absorption alone seems difficult to explain the variation. A third alternative is changes in the X-ray beaming direction, as suggested by the evidence of the superluminal motion (Alef et al. 1988). This alternative is, however, doubtful, because the radio lobes indicate a jet that is fairly stable on time scales of millions years and is not pointing toward us. We therefore presume that the long-term variability of 3C 390.3 is mainly due to intrinsic luminosity changes in the nonthermal radiation from the nucleus, possibly accompanied by an increase in the circumnuclear absorption as a secondary effect (e.g., through reduced photoionization flux).

Compared to the long-term variations, short-term variability seems to be a less clear phenomenon for this galaxy. This characteristic is rather commonly seen in other high-luminosity AGNs (e.g., Barr & Giommi 1992; Grandi et al. 1992; Williams et al. 1992; Ohashi et al. 1992). It is interesting

to consider here Centaurus A, which is also a double-lobed radio galaxy (at a $D \sim 5$ Mpc distance) but is two orders of magnitude less luminous than 3C 390.3. In fact, Cen A not only shows long-term large amplitude changes up to a factor of 30 or so (Morini, Anselmo, & Moltini 1989), but also a rapid intensity decrease by a factor of three within 5 minutes (Wang et al. 1986). Cen A is further distinguished from 3C 390.3 in that it exhibits a large X-ray absorption ($N_H \sim 10^{23}$ H atoms cm^{-2}) as well as much stronger iron fluorescence lines and is not an OVV. These differences between Cen A and 3C 390.3 are most naturally attributed to the difference in the intrinsic luminosity.

4.2. *Continuum Spectra and X-Ray Emission Mechanism*

The continuum X-rat spectra of 3C 390.3 obtained with *Ginga* are dominated by a nonthermal component, with rather tight upper limits on contribution from thermal emission (<5% of the total luminosity seen in *Ginga*). The photon indices Γ from the two *Ginga* observations are 1.77 ± 0.01 (average of the 2 days) and 1.54 ± 0.02, while all the measured *EXOSAT* spectra are consistent with Γ of 1.6–1.8. Spectral indices determined by earlier satellites (Halpern 1982; Rothschild et al. 1983; Barr et al. 1980; Mushotzky, Baity, & Peterson 1977) are generally consistent with these values, although subject to larger errors. Thus the X-ray spectra of 3C 390.3 are similar to those of other AGNs, including Seyfert galaxies, QSOs, and some BL Lac objects with flat-Xray spectra.

EXOSAT measurements of the spectral index are subject to too large error bars to search for any correlation between flux and spectral index. On the other hand, between the two *Ginga* observations separated by ~2 years, the X-ray spectrum of 3C 390.3 *flattened* as its 2–20 keV luminosity decreased from $(2.57 \pm 0.06)h^{-2}$ to $(1.62 \pm 0.05)h^{-2} \times 10^{44}$ ergs s^{-1}. This luminosity-spectrum correlation is reminiscent of the behavior of Seyfert galaxies, in which X-ray flux decrease is often, if not always, accompanied by spectral flattening (e.g., Pound et al. 1990; Matsuoka et al. 1990; Grandi et al. 1992). In QSOs and BL Lac objects, the X-ray spectrum on the contrary tends to become steeper as the source gets fainter (e.g., Makino et al. 1989; Sembay et al. 1992). In most other respects, however, 3C 390.3 does not resemble Seyfert galaxies. For example, the iron K-edge absorption feature and low-energy absorption, both quite common to the X-ray spectra of Seyfert galaxies, have not been detected in the 3C 390.3 spectra. In addition, the intense radio emission from the nucleus and from the lobes of 3C 390.3 provides the most outstanding difference of this object from Seyfert galaxies.

When 3C 390.3 is X-ray bright, its X-ray flux lies above the smooth extrapolation of radio-IR wide band spectrum (Fig. 6), thus bearing close similarity to radio-loud QSOs (e.g., Ohashi et al. 1992). It is therefore likely that a major fraction of X-rays from 3C 390.3 is emitted through the same mechanism as those from radio-loud QSOs. A favorite model in this case is synchrotron-self-Compton (SSC) mechanism; low-energy "seed" photons produced via synchrotron radiation by relativistic particles are Compton up-scattered into the X-ray region by the same electron population. The relatively slow X-ray variation observed from 3C 390.3 supports this picture, because the synchrotron cooling time of the electrons which emit soft seed photons (typically in the radio frequency) is expected to be quite long. Assuming that the electron spectrum is kept constant, we further expect that the spectral slope of the synchrotron component, hence of the self-Compton component too, depends on the change of the electron injection rate rather than the injection rate itself; when the injection rate increases, the spectrum flattens temporarily on time scales shorter than the relevant synchrotron cooling time. In other words, we should not expect unique relation between instantaneous X-ray intensity and spectral slope in the SSC scheme. The apparent spectral flattening observed in the fainter *Ginga* data may be manifestation of such a complex hysteresis between flux and spectrum.

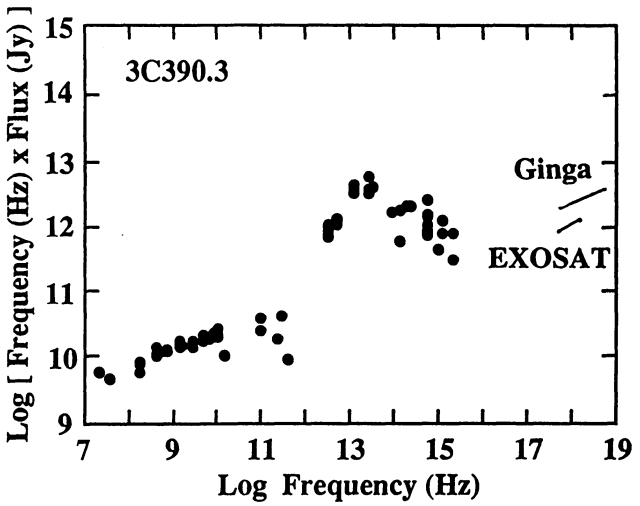

FIG. 6.—Wide-band spectrum of 3C 390.3. Radio and IR observations refer to Poggioli (1991), which are not simultaneous ones. Present *EXOSAT* (1984 day 153) and *Ginga* (1988 day 316–317) observations are also shown in the figure.

4.3. *Iron Line Emission*

We have obtained a firm evidence of iron K-line emission from 3C 390.3, with EW of order 100 eV, although we could not constrain the ionization state of iron. Previous iron line detections from high-luminosity AGNs have been limited to a few cases, including the radio-loud QSO 3C 273 (EW ~ 50 eV; Turner et al. 1990), the radio-quiet QSO 1821+643 (EW ~ 150 eV; Kii et al. 1991), and the broad-line radio galaxy 3C 382 (EW ~ 280 eV; Kaastra, Kuniera & Awaki 1991) whose luminosity was about one-fourth of the 1988 luminosity of 3C 390.3. Williams et al. (1992) obtained upper limits of order 100 eV on the iron line EW for about a dozen QSOs observed with *Ginga*. From Seyfert galaxies, iron lines have been observed much more commonly, with EW reaching 200 eV or more (Pounds et al. 1990; Matsuoka et al. 1990). These lines have been interpreted as due to fluorescence from cool and warm materials around the central continuum source. On the other hand, iron lines have not been observed from BL Lac objects and OVV quasars, and the obtained upper limits are sometimes as stringent as ~20 eV (Makino et al. 1989).

These results altogether suggest that iron line EW from these sources is inversely correlated to the continuum luminosity. This tendency has been investigated by Iwasawa & Taniguchi (1993), who call it "X-ray Baldwin effect." Although the interpretation is complex, for QSOs and radio galaxies the inverse correlation is likely to include the effect of continuum enhancement due to beamed emission. In this sense, the detection of iron line from 3C 390.3 with a moderate EW is reasonable, since the radio jets and the evidence of superluminal motion clearly indicate beamed emission for 3C 390.3 but the promi-

nent radio lobes indicate that the beam is not directly pointing toward us.

4.4. *Radio Lobe Confinement*

The *Ginga* observations have constrained the thermal X-ray luminosity of 3C 390.3 to be less than $1h^{-2} \times 10^{43}$ ergs s^{-1} in 2–20 keV, for thermal temperature of $kT < 10$ keV or $T < 1.2 \times 10^8$ K. This implies that any spherical and uniform hot gaseous halo around 3C 390.3, of an assumed radius R_{100} $\times$ 100 kpc and temperature $T_7 \times 10^7$ K must have electron density less than $2.8 \times 10 R_{100}^{-3/2} T_7^{-1/4} h^{-1}$ cm^{-3}. Here we use a relation that bolometric bremsstrahlung luminosity of a fully ionized hydrogen plasma with volume V (cm^3), temperature T (K), and uniform electron density n_e (cm^{-3}) is given as $10^{-26.6} n_e^2 V T^{1/2}$ ergs s^{-1} for $T \geq 10^7$ K. This constrains the thermal pressure of the halo to be less than $4 \times 10^{-11} R_{100}^{-3/2} T_7^{3/4} h^{-1}$ ergs cm^{-3}.

This limit is comparable to the hydrostatic pressure required to confine the radio lobes of 3C 390.3 calculated by Hargrave & McEllin (1975) based on the radio results, namely (2–6) $\times 10^{-10}$ and 2.4×10^{-11} ergs cm^{-3} for the south and north heads of the radio lobe, respectively. Thus we cannot make definite statement, either affirmative or negative, as to the case of hydrostatic confinement of the radio lobes by hot halo. However, Figure 5*a* gives an order of magnitude tighter limit on the thermal luminosity, if the hypothesized hot halo is cooler than $kT = 2$ keV as is usually the case for individual elliptical galaxies and poor clusters of galaxies. It therefore seems likely that some other mechanism, e.g., magnetic confinement, is operating in the radio lobes of 3C 390.3.

5. CONCLUSIONS

The radio galaxy 3C 390.3 was observed in X-rays by the *EXOSAT* and *Ginga* satellites over the period 1984–1991. The main results of these observations are as follows:

1. In the 2–20 keV energy band the source luminosity was found to be $L_X \sim 10^{44}$ ergs s^{-1}. Long-term X-ray time variability with a large amplitude (more than an order of magnitude) on a time scale of years was confirmed.
2. High-quality X-ray spectra were obtained, especially with *Ginga*. The continuum X-ray spectra obtained with *EXOSAT* and *Ginga* are well described with unabsorbed power-law model with the photon slope in the range 1.5–1.8. There was a change of slope between the two *Ginga* observations within an interval of $\sim$2 years; it flattened by $\sim$0.2 as its 2–20 keV luminosity decreased by $\sim$40%.
3. Iron K-emission line was for the first time detected from this source with the *Ginga* observations. The line EW was of order $\sim$100 eV. We could not determine the line origin within the error bars. Iron K-edge feature was not detected.
4. We derived upper limits on the thermal component from 3C 390.3 of less than $1h^{-2} \times 10^{43}$ ergs s^{-1} in 2–20 keV for thermal temperature of $kT < 10$ keV. This upper limit is not yet tight enough to completely exclude the confinement of the radio lobes by thermal pressure of extended hot gas.

We are grateful to the *Ginga* team members for continuous support. M. I. thanks R. Stern for his help in the search for the flare star candidate. G. G. C. P. acknowledges financial support from the Italian MURST and the Italian Space Agency (ASI) and Japan SPS for a travel grant. G. T. acknowledges financial support from ASI. This work was supported in part by NASA Contract NAS 8-39073 (ASC) and NASA grants NAGW-2681 (LTSA), NAGW-2681 (LTSA) and NAG 8-801 (*Ginga*).

REFERENCES

Alef, W., Gotz, M. M. A., Preuss, E., & Kellermann, K. I. 1988, A&A, 192, 53
Barr, P., & Giommi, P. 1992, MNRAS, 225, 495
Barr, P., et al. 1980, MNRAS, 193, 549
Barthel, P. D. 1989, ApJ, 336, 606
Brown, I. W. A., & Murphy, D. W. 1987, MNRAS, 226, 601
Burbidge, E. M., & Burbidge, G. R. 1971, ApJ, 163, L21
Caillaut, J.-P., Helfand, D. J., Nousek, J. A., & Takalo, L. O. 1986, ApJ, 304, 318
Canizares, C. R., Fabbiano, G., & Trichieri, G. 1987, ApJ, 312, 503
Charles, P. A., Longair, M. S., & Sanford, P. W. 1975, MNRAS, 170, 17
Clavel, J., & Wamsteker, W. 1987, ApJ, 320 L9
Elvis, M., Giommi, P., Wilkes, B. J., & McDowell, J. 1991, ApJ, 378, 537
Fabbiano, G., Kim, D. W., & Trinchieri, G. 1992, ApJS, 80, 531
Fanaroff, B. L., & Riley, J. M. 1974, MNRAS, 167, 31
Forman, W., Jones, C., Cominsky, L., Julien, P., Murray, S., Peters, G., Tananbaum, H., & Giacconi, R. 1978, ApJS, 38, 357
Forman, W., Jones, C., & Tuchker, W. 1985, ApJ, 293, 102
Giacconi, R., & Gursky, H. 1974, in X-Ray Astronomy, ed. R. Giacconi & H. Gursky (Dordrecht: Reidel), 397
Gioia, I. M., Maccacaro, T., Shild, R. E., Wolter, A., Stocke, J. T., Morris, S. L., & Henry, J. P. 1990, ApJ, 72, 567
Grandi, P., Tagliaferri, G., Giommi, P., Barr, P., & Palumbo, G. G. C. 1992, ApJS, 82, 93
Haish, B. M. 1983, in Activity in Red-Dwarf Stars, ed. P. B. Byrne & M. Rodono (Dordrecht: Reidel), 255
Halpern, J. P. 1982, Ph.D. thesis, Harvard University
Hargrave, P. F., & McEllin, M. 1975, MNRAS, 173, 37
Hayashida, K., et al. 1989, PASJ, 41, 373
Heiles, C., & Habing, H. J. 1974, A&AS, 14, 1
Iwasawa, K., & Taniguchi, Y. 1993, ApJL, in press
Kaastra, J. S., Kunieda, H., & Awaki, H. 1991, A&A, 242, 27
Kii, T., et al. 1991, ApJ, 367, 455
Laing, R. A., Riley, J. M., & Longair, M. S. 1983, MNRAS, 204, 151
Lloyd, C. 1984, MNRAS, 209, 697
Makino, F., et al. 1989, ApJ, 347, L9
Marshall, F. E., Mushotzky, R. F., Boldt, E. A., Holt, S. S., Rothschild, R. E., & Serlemitsos, P. J. 1978, Nature, 275, 624
Matsuoka, M., Piro, L., Yamauchi, M., & Murakami, T. 1990, ApJ, 362, 440
Morini, M., Anselmo, F., & Molteni, D. 1989, ApJ, 347, 750
Mushotzky, R. F. 1984, Adv. Space. Res., Vol. 3, Nos. 10–12, 157
Mushotzky, R. F., Baity, W. A., & Peterson, L. E. 1977, ApJ, 212, 22
Ohashi, T., Tashiro, M., Makishima, K., Kii, T., Makino, F., Turner, M. J. L., & Williams, O. R. 1992, ApJ, 398, 87
Oke, J. B. 1986, in Superluminal Radio Sources, ed. J. A. Zensus & T. J. Pearson (Cambridge Univ. Press), 267
Orr, M. J. L., & Brown, I. W. A. 1982, MNRAS, 200, 1067
Pallavicini, R., Tagliaferri, G., & Stella, L. 1990, A&A, 228, 403
Penston, M. V., & Penston, M. J. 1973, MNRAS, 162, 109
Perez, E., Penston, M. W., Tadhunter, C., Mediavilla, E., & Moles, M. 1988, MNRAS, 230, 353
Poggioli, M. 1991, M.A. in Astronomy, University of Bologna
Pounds, K. A., Nandra, K., Stewart, G. C., George, I. M., & Fabian, A. C. 1990, Nature, 344, 132
Raymond, J. C., & Smith, B. W. 1977, ApJS, 35, 419
Rothenflug, R., & Arnaud, M. 1985, A&A, 144, 431
Rothschild, R. E., Mushotzky, R. F., Baity, W. A., Gruber, D. E., Matteson, J. L., & Peterson, L. E. 1983, ApJ, 269, 423
Sembay, S., et al. 1993, ApJ, 404, 112
Shafer, R., Ward, M., & Barr, P. 1985, Space Sci. Rev., 40, 637 (SWB85)
Tsuru, T., et al. 1989, PASJ, 41, 679
Turner, M. J. L., et al. 1989, PASJ, 41, 345
———. 1990, MNRAS, 244, 310
Turner, M. J. L., Smith, A., & Zimmerman, H. U. 1981, Space Sci. Rev., 30, 513
Turner, T. J., & Pounds, K. A. 1989, MNRAS, 240, 833
van Breugel, W., & Jagers, W. 1982, A&AS, 49, 529
Wamsteker, W., & Clavel, J. 1989, IAU Circ., No. 4763
Wang, B., Inoue, H., Koyama, K., Tanaka, Y., Hirano, T., & Nagase, F. 1986, PASJ, 38, 685
Williams, O. R., et al. 1992, ApJ, 389, 157
Wood, K. S., et al. 1984, ApJS, 56, 507